New evidence for millennial-scale interactions between Hg cycling and hydroclimate from Lake Bosumtwi, Ghana

Alice R. Paine[1]*, Joost Frieling[1], Timothy M. Shanahan[2], Tamsin A. Mather[1], Nicholas McKay[3], Stuart A. Robinson[1], David M. Pyle[1], Isabel M. Fendley[1], Ruth Kiely[4], William D. Gosling[4]

[1]Department of Earth Sciences, University of Oxford, UK, OX1 3AN
[2]Department of Earth and Planetary Sciences, University of Texas at Austin, Texas, USA
[3]School of Earth and Sustainability, Northern Arizona University, Flagstaff, Arizona, USA
[4]Institute for Biodiversity & Ecosystem Dynamics, University of Amsterdam, Amsterdam, Netherlands

Corresponding Author: alice.paine@earth.ox.ac.uk

SUPPLEMENTARY INFORMATION

S1. BOS04-5B core details

Extraction of the BOS04-5B sediment succession took place between July and October of 2004#. Drill sites were chosen following a series of geophysical, seismic, and limnological studies conducted between 2000-2002 , and drilling operations divided into two main parts: sediment (first two months), and the hard-rock (impactite and bedrock)(Karp et al., 2002; Koeberl et al., 2007b, 2005). Drilling was performed using the DOSECC/ICDP GLAD800 system custom-built specifically for lake drilling, from which twenty-three sediment cores, and two hard-rock (impactite) cores were obtained in the course of the 2004 ICDP drilling project (full details in Koeberl et al.(Koeberl et al., 2005)). This study focuses on the upper ~47 m section of a 296-m-long core extracted from deep-water (76 m) site 5 (core BOS04-5B). The core extends from the present-day lake floor to the brecciated bedrock, includes a basal sediment layer of impact-glass bearing accretionary lapilli with a thickness of ~30 cm, and has been dated by $^{40}Ar/^{39}Ar$ to 1.08±0.04 Ma(Jourdan et al., 2009).

After drilling, the cores were shipped to the University of Rhode Island, where they were split, described, imaged, and analysed using a Geotek® multi-sensor core logger for a suite of magnetic and physical parameters. The cores were sampled for analysis of sediment magnetic hysteresis, x-ray diffraction mineralogy, total organic and inorganic carbon content, bulk organic carbon and nitrogen isotopes, and grain size. Core logging and physical sediment properties were used to develop a standardized depth scale for core 5B: permitting comparison between holes (e.g., site 5b and 5c) and coring locations (e.g., site 4, site 5)(Shanahan et al., 2013). Core depths presented in this paper are in meters below lake floor.

S2. Sample preparation

Studies report a range of techniques to dry lacustrine sediments in preparation for Hg analyses, which include freeze-drying (Daga et al., 2016; Guédron et al., 2019; Hermanns and Biester, 2013; Ribeiro Guevara et al., 2010), high-temperature (Pérez-Rodríguez et al., 2019), and low-temperature oven drying (de Lacerda et al., 2017; Gelety et al., 2007). To determine if/how heat exposure may affect sedimentary concentrations of Hg in soft recent lacustrine sediments such as those from BOS04-5B, a pilot study was conducted using externally sourced, homogenous material. Approximately 14cm^3 of soft, muddy material was separated and subjected to different drying conditions. Samples (in triplicate) were dried at three temperatures, respectively: groups E1 and E3 at 40°C (oven), group E2 at 100°C (oven), and group C1 at -50°C (freeze dryer). Exposure times were also systematically varied between samples, ranging from one day (E2), to 1 week (E1 and C1), and four weeks (E3). Once dry, samples were ground using a mortar and pestle to produce a homogenous powder, and six Hg analyses (method described in section 3.4) were conducted for each group with three vials run as duplicates.

Our results showed a weak correlation between exposure temperature and Hg concentration (r^2 = 0.09). The lowest mean Hg concentrations were measured in the samples dried at 100°C, which could allude to Hg release during heating. Nonetheless, the results suggest that drying temperature does not strongly affect sedimentary Hg concentrations, with mean values across all four groups ranging from 27–30 ng g^{-1}. Following these results, BOS04-5B samples were prepared by oven-drying at 30°C for 72 hours before grinding the sediment to powder form, as this presented the quickest, least resource-intensive option and posed no risk of Hg loss.

S3. Chronology

The BOSMORE7 model (Gosling et al., 2022) provides a newer, updated age-depth relationship for the BOS04-5B core compared to those earlier presented by Shanahan et al. (2013) and Miller et al. (2016). First, because it integrates the ^{39}Ar/^{40}Ar-derived crater age of 1.07±0.11 Ma (Jourdan et al., 2009; Koeberl et al., 1997) to generate more robust age uncertainties for the deeper core sections. Second, because it does not include the six paleomagnetic excursions (Mono Lake, Laschamp, 4-a, 5-a, 5-b, 6-a) previously used as tie-points, owing to uncertainties in the reliability of these dates (Gosling et al., 2022). An age-depth relationship was constructed using a Bayesian approach in R, from which the model provided an ensemble of possible age models, their analytical age uncertainties, and sedimentation rates (Blaauw and Christen, 2011). The code a used in model generation is available from: https://doi.org/10.6084/m9.figshare.18319466).

S4. Mercury measurements

Total Hg (Hg_T) in the bulk sediments of core BOS04-5B was measured using the RA-915 Portable Mercury Analyzer with PYRO-915+ Pyrolyzer, Lumex (Bin et al., 2001) at the University of Oxford. For this study, we analysed 165 samples spanning the composite depth interval 47.7 to 0 m, with an average temporal resolution of ~0.6 ka between each sample. Dry powdered sample material (45–100 mg) was heated to ~700ºC, volatilizing Hg in the sample. Atomic absorption spectrometry of the gases produced during pyrolysis quantifies the total Hg content of the sample. Six different quantities of standard material (paint-contaminated soil – NIST Standard Reference Material ® 2587) with a known Hg value of 290 ± 9 ng g^{-1} were run to calibrate the instrument before sample analysis, and then one standard for every 10 lacustrine samples (calibration results in **supplementary file**). Long-term observations of standard measurements *(n* = 390*)* for this instrument indicate single-side reproducibility around 6% for samples with ≥10 ng g^{-1} Hg (Frieling et al. 2023). Four (2%) of the analysed samples contained very low Hg contents (<10 ng g^{-1}), and so have uncertainties >10 %. Recovery of the Hg volatilized from each sample run by pyrolysis-based instrumentation is assumed to be 100%, as expected from pyrolysis-based instrumentation for these types of rock powders (Bin et al., 2001).

S5. TOC measurements

To measure TOC contents of the BOS04-5B succession, powdered sediment samples were split into two aliquots and weighed. Weights for aliquot 1 were between 50-70 mg, and aliquot 2 between 90-120 mg. Prior to coulometric analysis, samples in aliquot 2 were furnaced for 24 hours at 420°C in order to remove organic carbon fractions. Both aliquots were then combusted in oxygen at 1220 °C to break down the calcium carbonate and produce carbon dioxide (CO_2), which was fed into a solution of barium perchlorate. This would result in a change in the solution pH from an initial value of 10.0, following which back titration to the original pH using electrolysis gives a measure of the amount of carbon originally present – quantified by the amount of electricity required to restore a pH of 10.0, and recorded in counts (Jenkyns, 1988; Jenkyns and Weedon, 2013). Counts obtained for Aliquots 1 and 2 were used to calculate the total carbon (TC) content of the sample in wt.%, using the formula:

$$TC = \frac{total\ counts\ x\ 0.2}{M} \qquad \textit{(eq. 1)}$$

…whereby M is the sample mass in mg.

TOC were calculated as:

$$TOC = TC_1 - TC_2 \qquad \textit{(eq. 2)}$$

… whereby TC_1 and TC_2 represent the TC values obtained for aliquots (1) and (2), respectively.

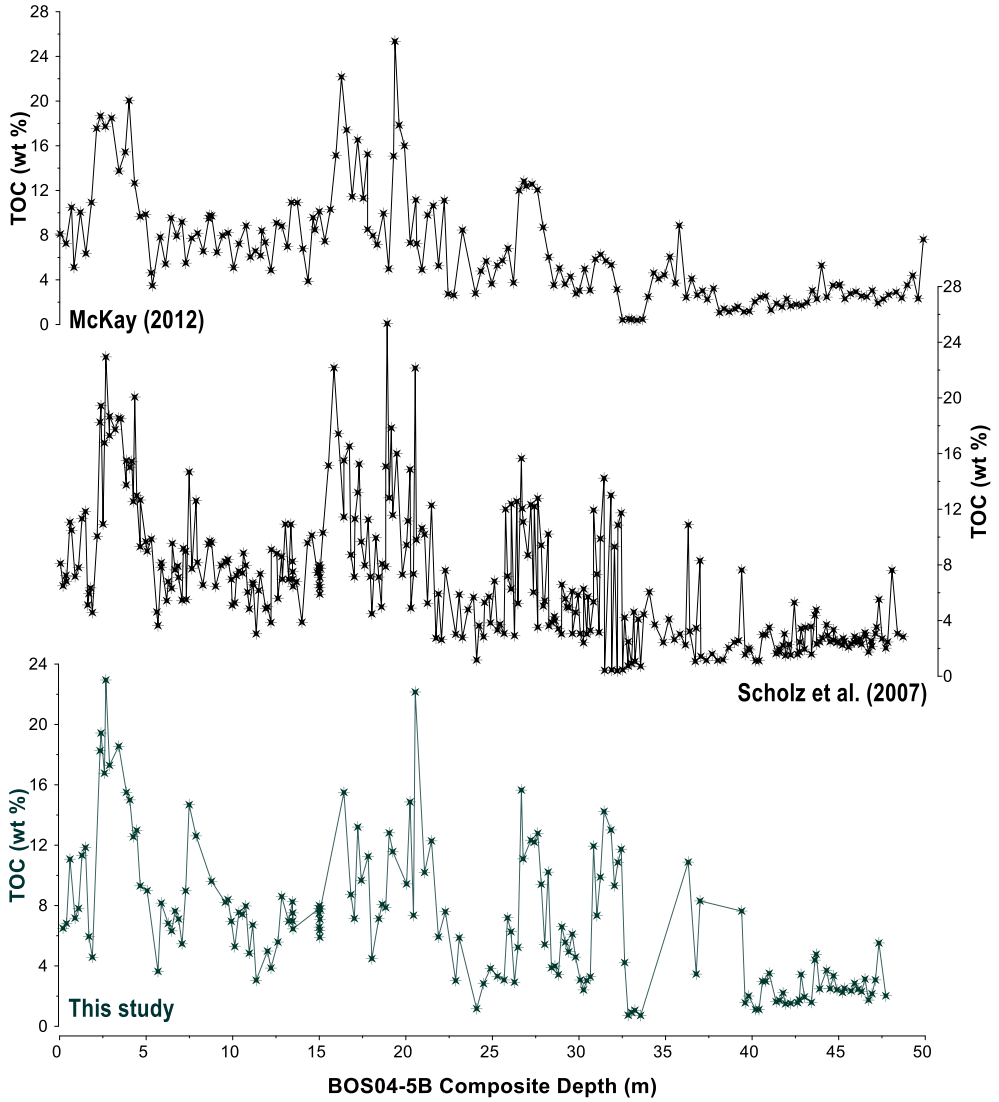

Figure S1: A comparison of TOC datasets for the upper 47 m of core BOS04-5B, obtained by loss-on-ignition (McKay, 2012; Scholz et al., 2007), and coulometry (*this study*). Sampling points are marked by stars on all three plots.

S6. Authigenic carbonates

The BOS04-5B succession contains variable amounts of diagenetic carbonates, predominantly (mangano-) siderite (**Fig. S1a**) (McKay, 2012). Siderites commonly form in freshwater settings at shallow sediment depths under anaerobic (anoxic) conditions accompanied by organic-rich sediments (Armenteros, 2010; Sebag et al., 2018). The siderite-bearing intervals in the core can be easily identified using bulk chemistry (e.g., XRF data) as Mn-enriched intervals, as Mn is unlikely to be a significant component of other sedimentary minerals. However, accurate measurement of organic carbon content in lacustrine sediment via pyrolysis- or furnace-based methods can be challenging in the presence of siderite. Thermal decomposition of siderite typically starts at temperatures <420^{o}C (Sebag et al., 2018), which is lower than that which is used to remove the organic fraction on the

Coulomat (Jenkyns, 1988). Consequently, the released siderite-sourced carbon would lead to systematic overestimation of total organic carbon (Sebag et al., 2018).

To assess whether siderite-associated carbon had an appreciable impact on the TOC measurements, we measured the carbon release from siderite using repeat analyses of a Jurassic-age siderite nodule (~ 85% siderite by weight, n=4). Siderite decomposition (carbonate-carbon loss) was near-complete (>95%) after furnacing overnight at 420 ºC, so that it can be assumed that all siderite carbon in the Bosumtwi material was measured as “TOC”. We therefore removed siderites from sixteen BOS04-5B samples spanning a range of low-high Mn counts using a weak acid (warm 5% HCl) treatment, following established methodologies (Brodie et al., 2011; Vindušková et al., 2019) (full details in **S4**). We then compared acid-treated and furnaced samples to assess the impact on TOC measurements for Bosumtwi sample material. The difference between untreated and treated samples ranged between -1.6 % and 1.38 %, which aligns with the expected difference between acid-treatment and pyrolysis-based methods for very organic-rich sediments. There was, however, no systematic offset nor a clear correlation with the Mn counts from XRF data (**Fig. S1c**), suggesting that the carbon release from siderite did not appreciably bias TOC measurements.

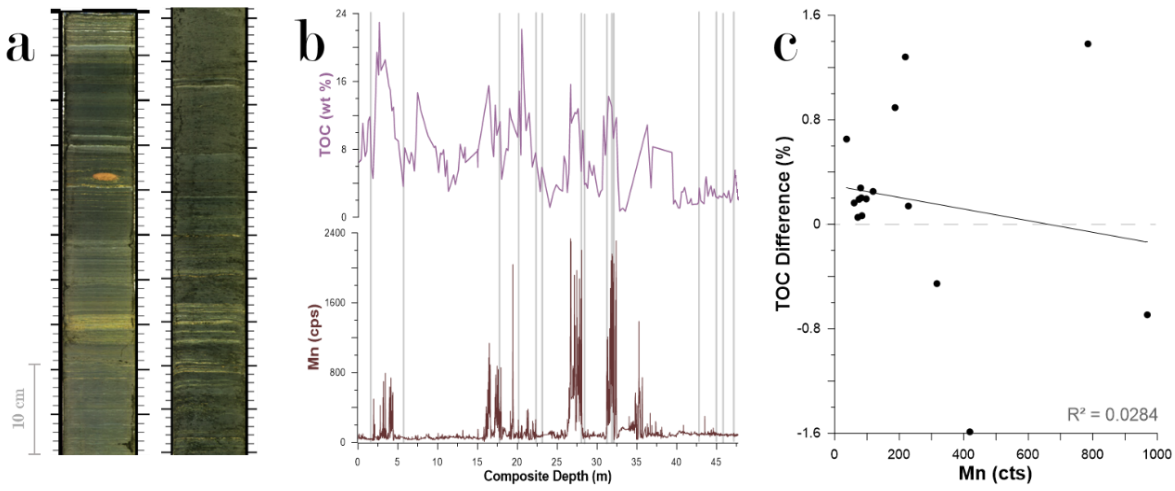

Fig. S2: (a) Scan images of select sections of core BOS04-5B from Lake Bosumtwi, showing clear yellow-white carbonate layers. (b) Comparison of Mn abundance(McKay, 2012) and total organic carbon (TOC) (*this study*) data. (c) Relationship between Mn abundance, and the difference between TOC_U and TOC_T.

S7. Scanning X-Ray fluorescence

The Hg data for core BOS04-5B generated in this study are paired with unpublished x-ray fluorescence (XRF) data (McKay, 2012), obtained from analyses conducted on the upper ~159 m (~500-kyr) of BOS04-5B. Bulk elemental abundance was analysed using the Itrax® scanning x-ray fluorescence (XRF) analyser at the Large Lake Observatory at the University of Minnesota, Duluth. The archive halves of split sediment cores were analysed at 1-cm-resolution, with 60 sec count times

and a Mo x-ray source operated at 30 kV and 20 mA. Digital x-radiographs with 200-µm-resolution in the downcore direction for each of the core segments were also generated using this instrument

Scanning XRF analysis of wet, split sediment cores can be affected by a number of factors when applied over highly variable lithologies; as are present in BOS04-5B (McKay, 2012). To correct for changes in sediment water content and compaction of the core with depth, XRF data were corrected using the known mass attenuation constants of the different elements to calculate the impact of x-ray absorption and scattering by water (Kido et al., 2006). Bulk sediment composition of BOS04-5B was estimated by simple 3-point calibrations with standard reference materials (SRMs), and water content calculated from the dry and wet bulk densities measured on the Geotek Core Scanner, and by loss-in-ignition, respectively (McKay, 2012). This calibration likely overestimates the water content at the time of measurement, since water content values used for calibration were measured immediately after the core was split, whereas the XRF data were collected several years later; meaning that the cores had dried somewhat during storage. Estimated drying of ~30% is justified on the basis of comparison between the cores at the time of XRF analysis and core photos taken after splitting. Hence, original water content values were multiplied to yield ~ 80% wet bulk density.

Unconsolidated lacustrine sediment compacts as a function of the increasing weight of overlying material with depth, producing a downcore increase in density and decrease in porosity that changes most rapidly near the surface (Bahr et al., 2001). Given the high lithological variability in BOS04-5B, traditional methods for compaction correction (e.g., fitting an exponential, logarithmic, or low-order polynomial) would produce a compaction curve that either overfits the data, or poorly fits the upper ~50 m. Therefore, a piecewise approach was taken for BOS04-5B in which a 2nd and 1st order polynomial was fitted to the data using a non-parametric algorithm, and the fit of this curve was subsequently divided by the XRF intensities (McKay, 2012).

SUPPLEMENTARY DISCUSSION

S8. Variations in Hg host phases with time

Time-resolved variability in the degree of covariation between Hg, TOC, and detrital matter was explored by means of a simple rolling-window (RW) correlation analysis, which has been highlighted as an effective tool for exploration of compositional variability through time (Oehlert and Swart, 2019; Sun et al., 2021; Ulfers et al., 2022; Wang et al., 2014). Applying this technique to the BOS04-5B Hg data permits a broad assessment of variability in Hg host-phase relationships in this system through time, identify any measurable changes that could reflect major changes in Hg burial dynamics, and elucidate the potential mechanisms responsible for these changes. Once Pearson correlation coefficients between the Hg, TOC, and K data had calculated, time series profiles were then averaged across two window sizes - ~1-kyr and ~10-kyr – and presented in **Figure S2**.

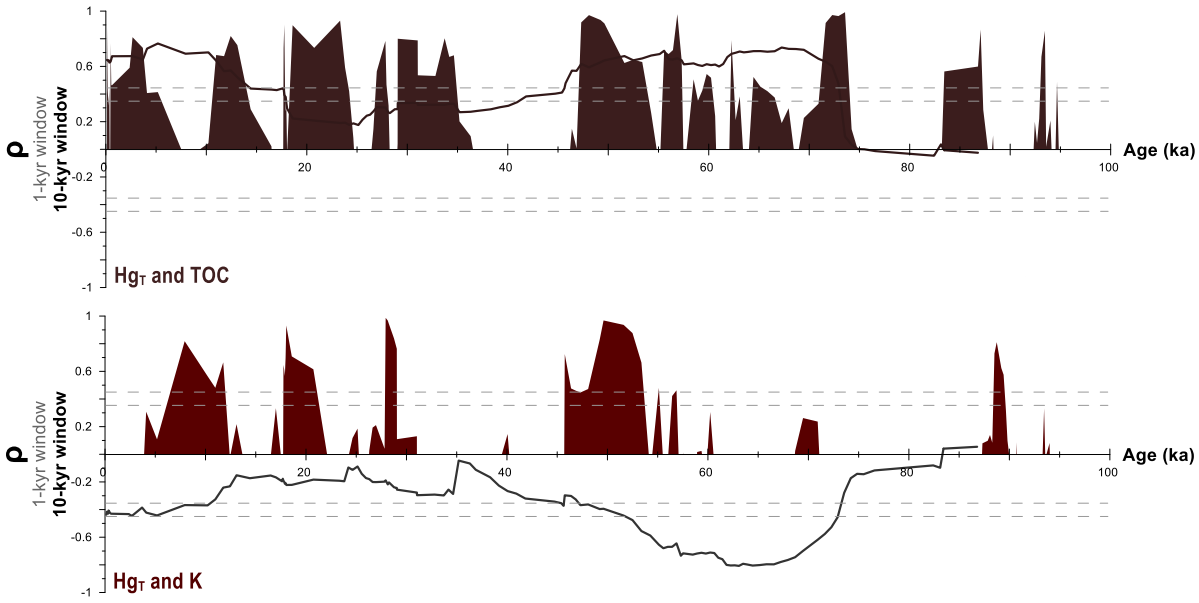

Figure S3: Pearson's correlation coefficients (ρ) between total Hg (Hg$_T$) and potassium (K), and Hg$_T$ and organic matter (TOC) data from core BOS04-5B from Lake Bosumtwi. Significance bands are marked with dashed grey lines (± 20%), and shaded areas indicate periods of high correlation where R values exceed the upper limit of this threshold. A ~1-kyr window size corresponds to a stratigraphic resolution of ~1 m, and a ~10-kyr window size to a stratigraphic resolution of ~10 m.

The Hg and TOC relationship identified by linear correlation analysis (**Fig. S3**) appears consistently positive throughout the succession. Focussing on the ~10-kyr series, R values typically range between ~0.9 and 0.2 with only transient instances where this value drops <0.2. Conversely, the Hg/K profile shows a consistently negative relationship between Hg$_T$ and the detrital fraction in BOS04-5B (**Fig. S3**), which fluctuates in an antithetical manner to the Hg and TOC profile. For example, the weakest correlation between Hg and the detrital fraction is observed when the Hg and TOC relationship is strongest between ~73 and 45 ka (**Fig. S3**). Nonetheless, a common feature between the two plots is a broad downward trend in the correlation coefficients through time, with the highest values generally observed in the deeper (older) core sections (**Fig. S3**). Variability through time is

significantly more pronounced for the ~1-kyr-window profiles. Sporadic, high-amplitude peaks at discrete points throughout the record show transient instances whereby the correlation between Hg, organic matter and/or detrital influx changes measurably, suggesting that Hg signals recorded in Lake Bosumtwi since ~100 ka could also reflect changes in the net flux of Hg into the system, and not solely host phase availability.

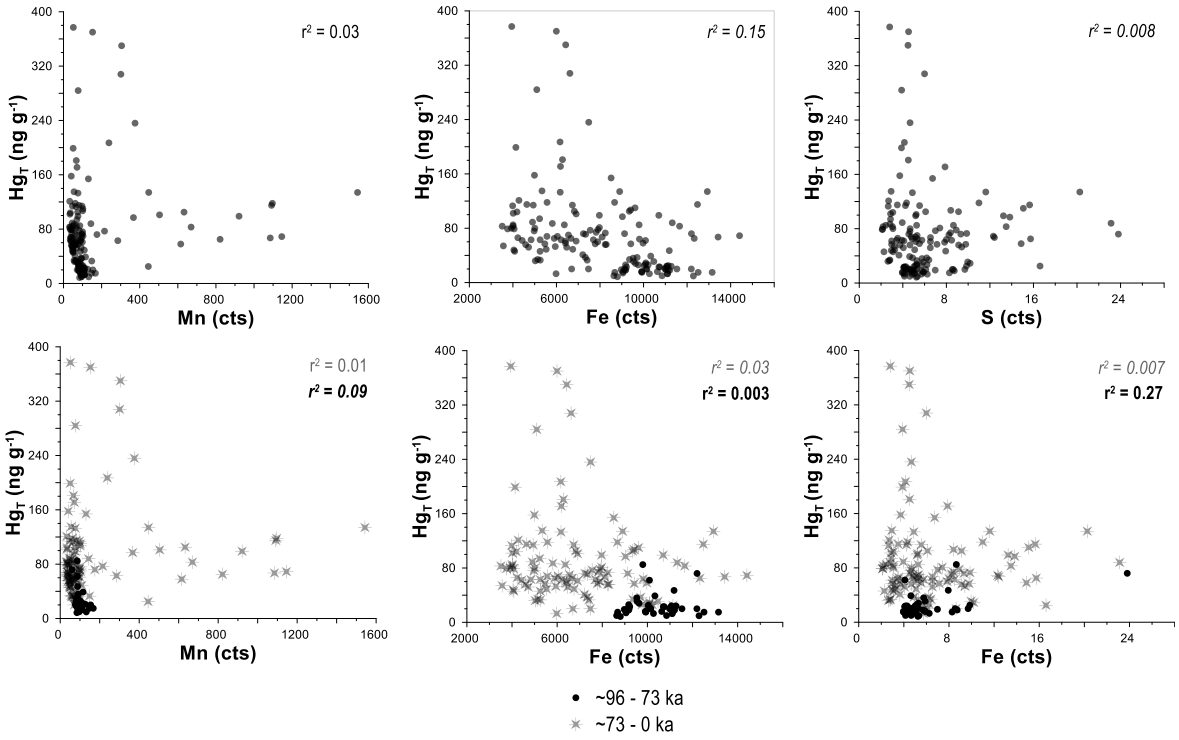

Figure S4: Comparison of relationships between Hg_T and manganese (Mn), Hg_T and iron (Fe), and Hg_T and sulphur (S) in core BOS04-5B. In the lower two plots, we separate datasets into two intervals: ~96 to 73 ka (black circles), and ~73 to 0 ka (grey stars). Mn, Fe, and S data were measured using XRF by McKay (2012). R-squared (r^2) values for each interval are also given, with italic formatting indicating a negative relationship.

S9: Detrital materials

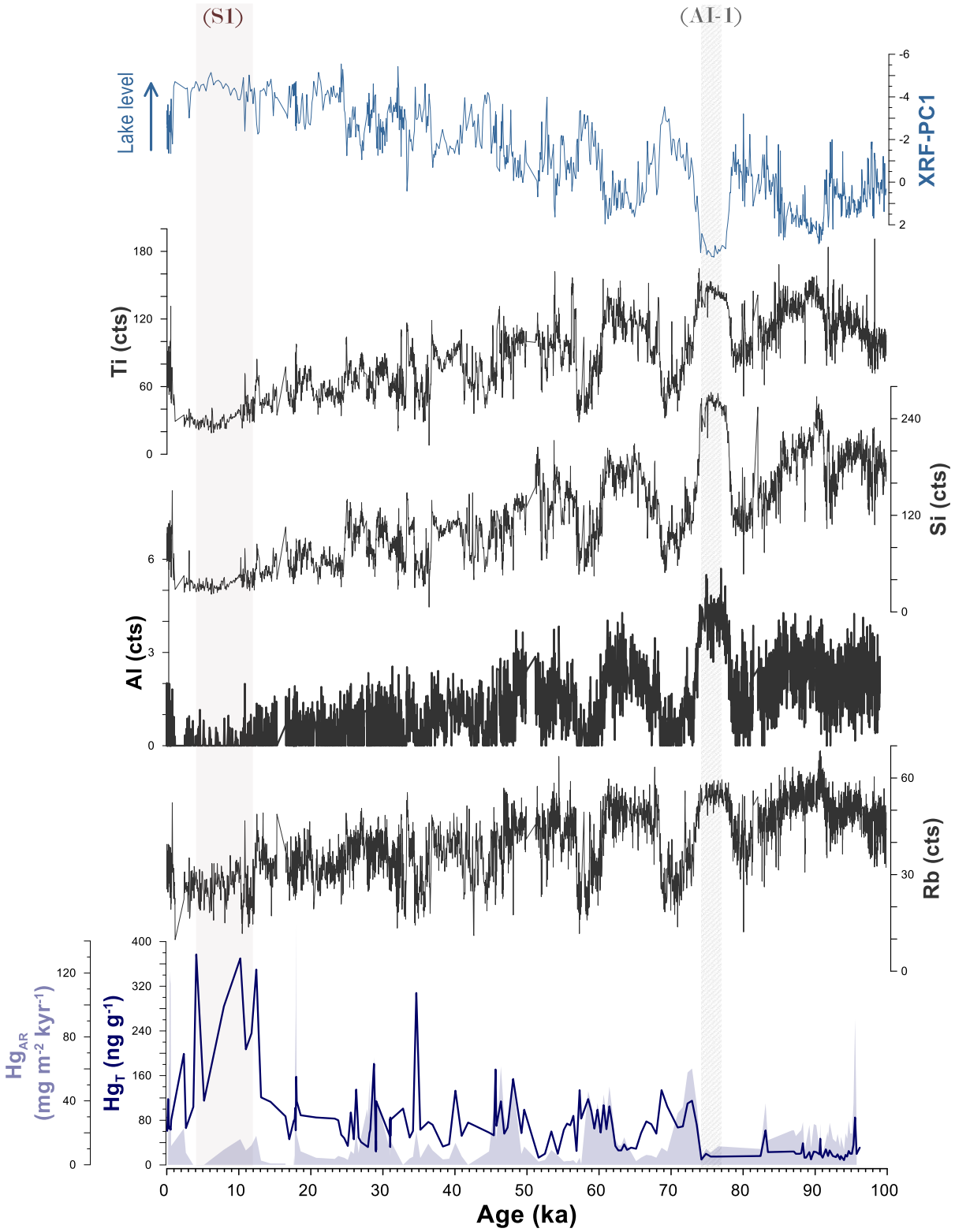

Figure S5: Records of Hg_T and Hg_{AR} (this study) for the upper ~47 m of core BOS04-5B, compared with X-ray fluorescence data obtained by McKay (2012), signaling changes detrital material influx into the basin.

S10. Sapropels

Table S1: Age boundaries and durations of sapropels identified in core LC21 from the Mediterranean Sea, and timing of the respective African monsoon signal. Sapropels corresponding to the interval of focus in this study (and displayed in **Figure 5** (*main text*)) are highlighted in grey, with 'ka' representing thousand years before present. Table adapted from Grant et al., (2016)

Sapropel	Start (ka)	End (ka)	Duration (kyr)	Monsoon signal (ka)
1	6.1	10.5	4.4	10.8
3	80.8	85.8	5	85.8
4	101.8	107.8	6	108
5	121.5	128.3	6.8	128.3

Table S2: Details of proxy records displayed in **Figure 5**

Core	Location	Latitude	Proxy	Interpretation	Reference(s)
GeoB7920	Atlantic Ocean	20°N	Humidity Index (HI)	Grain-size distribution of the siliciclastic sediment fractions were used to derive proportions of three statistically relevant endmembers: coarse aeolian dust (EM1), fine aeolian dust (EM2), and hemi-pelagic mud (EM3). EM3 can be related to fluvial transport, and the proportions of aeolian endmembers EM1 and EM2 to subaerial erosion and vegetation cover. Authors use the log ratios of EM3, EM1 and EM2 (log[EM3/(EM1 + EM2)]) to derive an index reflecting relative changes of the continental humidity and vegetation cover.	(Tjallingii et al., 2008)
ODP 927	Mediterranean Sea	34°N	Ti/Al	Ti/Al in the open Eastern Mediterranean reflects relative variations in North African aeolian vs riverine inputs to the basin. Aeolian-sourced Ti/Al in the open Eastern Mediterranean is enhanced relative to fluvially-sourced Ti/Al because heavier (Ti-bearing) suspended particles preferentially settle near the Nile fan. Al normalisation (for Ti and Ba) also removes closed-sum effects. Higher values signal an aeolian source, lower values signal a fluvial source.	(Grant et al., 2022, 2017)
ODP658	Atlantic Ocean	20°N	Dust fluxes	Reflects aeolian (mineral) dust export from the Sahara desert, and broader variations in wind strength, wind speed, African monsoon intensity, humidity, and atmospheric circulation dynamics.	(Kinsley et al., 2022)
MD03-2705	Atlantic Ocean	18°N	Dust fluxes	Reflects aeolian (mineral) dust export from the Sahara desert, and broader variations in wind strength, wind speed, African monsoon intensity, humidity, and atmospheric circulation dynamics.	(Skonieczny et al., 2019)
MD03-2621	Cariaco Basin	10°N	Reflectance (L*)	Sediment reflectance as a proxy for terrigenous sediment deposition into the ocean. Light/dark coloured laminations capture seasonally varying sediment inputs into the basin, modulated by ITCZ dynamics.	(Deplazes et al., 2013)
MD03-2707	Gulf of Guinea	2°N	Sea-surface temperature	Large-scale changes in West African monsoon precipitation and riverine runoff are reflected in the isotopic and barium (Ba) composition of seawater and budget of dissolved Ba in Gulf of Guinea which is, in turn, archived in microfossils that accumulate in marine sediments.	(Weldeab et al., 2007)

S11. Crater origin and geology

The Bosumtwi crater was formed by an asteroid impact 1.08 ± 0.04 Ma ago (Jourdan et al., 2009; Koeberl et al., 1997). Evidence for low shock metamorphism and impact melt fragment abundance in Bosumtwi crater-sourced samples suggests the majority of heavily shocked material was ejected from the crater (Coney et al., 2007; Koeberl et al., 2007a), with evidence for distal material ejection ~300 km away from the crater (Koeberl et al., 2007a, 1997), and up to ~800 m intra-basin uplift during the impact (Scholz et al., 2007). This substantial vertical displacement of material during the event may have included the excavation and emission of large quantities of geogenic Hg at the surface, including Hg vaporized and emitted immediately following impact (Artemieva et al., 2017; Feignon et al., 2022).

Quantitative estimates suggest that ~94,000–480,000 Mg Hg was emitted at the Earth's surface following the Chicxulub impact event (Artemieva et al., 2017; Fendley et al., 2019), and lithostratigraphic evidence for toasting of shocked quartz in the Bosumtwi crater suggest that the target rocks were particularly volatile-rich (Coney et al., 2007; Koeberl et al., 2007b). It is possible that the impact event resulting in formation of the crater resulted in mobilization and emission of geogenic Hg into the environment, however the extent to which the geogenic Hg pool may contribute to signals recorded in Lake Bosumtwi is difficult to constrain, owing to the age of the impact itself. Moreover, impact breccias extracted from the basin show no measurable evidence for a meteoritic component in the Bosumtwi crater (Koeberl et al., 2007b), meaning that the Hg concentration of the Bosumtwi impactor remains unconstrained, and it is therefore unlikely that the impactor itself would represent a significant source of the Hg measured in our record.

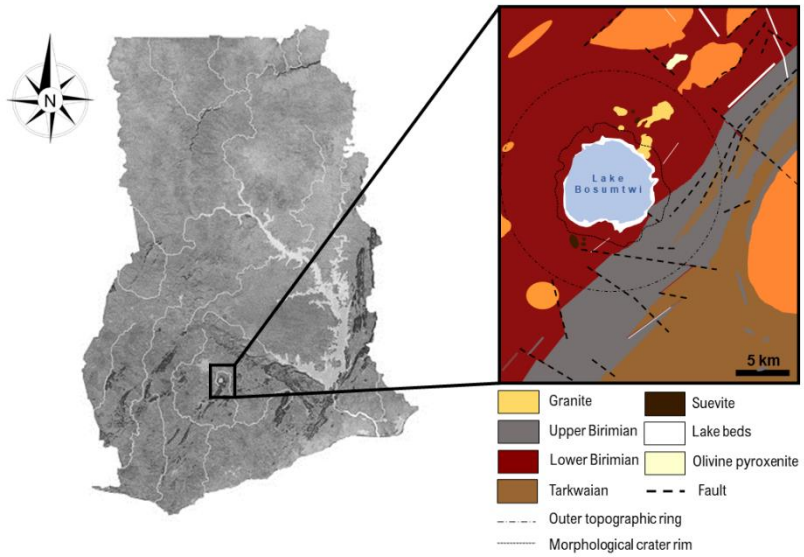

Figure S6: A schematic geological map of the Bosumtwi impact structure, Ghana. Adapted from Koeberl et al. (2007)

S12. Regional volcanism

Volcanic activity is a key component of the global Hg cycle (Pyle and Mather, 2003). Mobilization of geological Hg from deep Earth reservoirs to the surface occurs predominantly through diffuse emission of water vapour or geothermal gases during weathering and soil degassing, volcanism, and/or the erosion of Hg-bearing rocks (Fitzgerald and Lamborg, 2013; Rytuba, 2003; Selin, 2009). Thus, higher natural Hg concentrations in soil, air and bedrock found predominantly at or surrounding plate boundaries where tectonic, volcanic, and geothermal activities are most intense (Edwards et al., 2021; Rytuba, 2003; Schlüter, 2000). There are no active volcanoes in Ghana, however, Lake Bosumtwi is located in close proximity to several highly productive volcanic regions. For example, the East African Rift Zone contains ~20 major caldera structures with known histories of high-magnitude, explosive activity (Biggs et al., 2021; Pyle, 1999; Vidal et al., 2022), and other notable regions include the Cameroon Volcanic Line (CVL), the Canary Islands, and Cape Verde (Pyle, 1999). Identification

of cryptotephra produced by the ~74 ka eruption of Toba volcano (Indonesia) in Lake Malawi also highlights the potential for deposition of volcanogenic material over Africa originating from distal, exceptionally large eruptions (Lane et al., 2013).

The resolution of BOS04-5B precludes our ability to examine Hg emissions with respect to single eruption events. **Figure S7** does show a coincidence between the frequency of tropical volcanism and intervals of elevated Hg concentration in Lake Bosumtwi, however, it is likely that this is a function of disproportionately better volcanic records coinciding with these intervals. Eruption chronologies in Africa are compromised by a known lack of quantitative radiometric dates for many known Late Pleistocene events, owing to poor terrestrial preservation and limited sampling (Colby et al., 2022; Fontijn et al., 2018; Vidal et al., 2022). The same applies to volcanism in the Northern Hemisphere low-latitudes, with record incompleteness linking to strong erosion and vegetation regrowth favoured by tropical climates, coupled with spatial differences in sampling frequency (Brown et al., 2014). Improvements in eruption recording also coincide with a global rise in Hg emissions resulting from industrial practices during the Holocene (United Nations Environment Programme, 2018), which could further increase wet deposition of Hg in the terrestrial realm. Taken together, eruption record incompleteness coupled with time-transgressive changes in the global atmospheric Hg burden both complicate the ability to unambiguously correlate enhanced volcanic emissions to greater Hg deposition in our record.

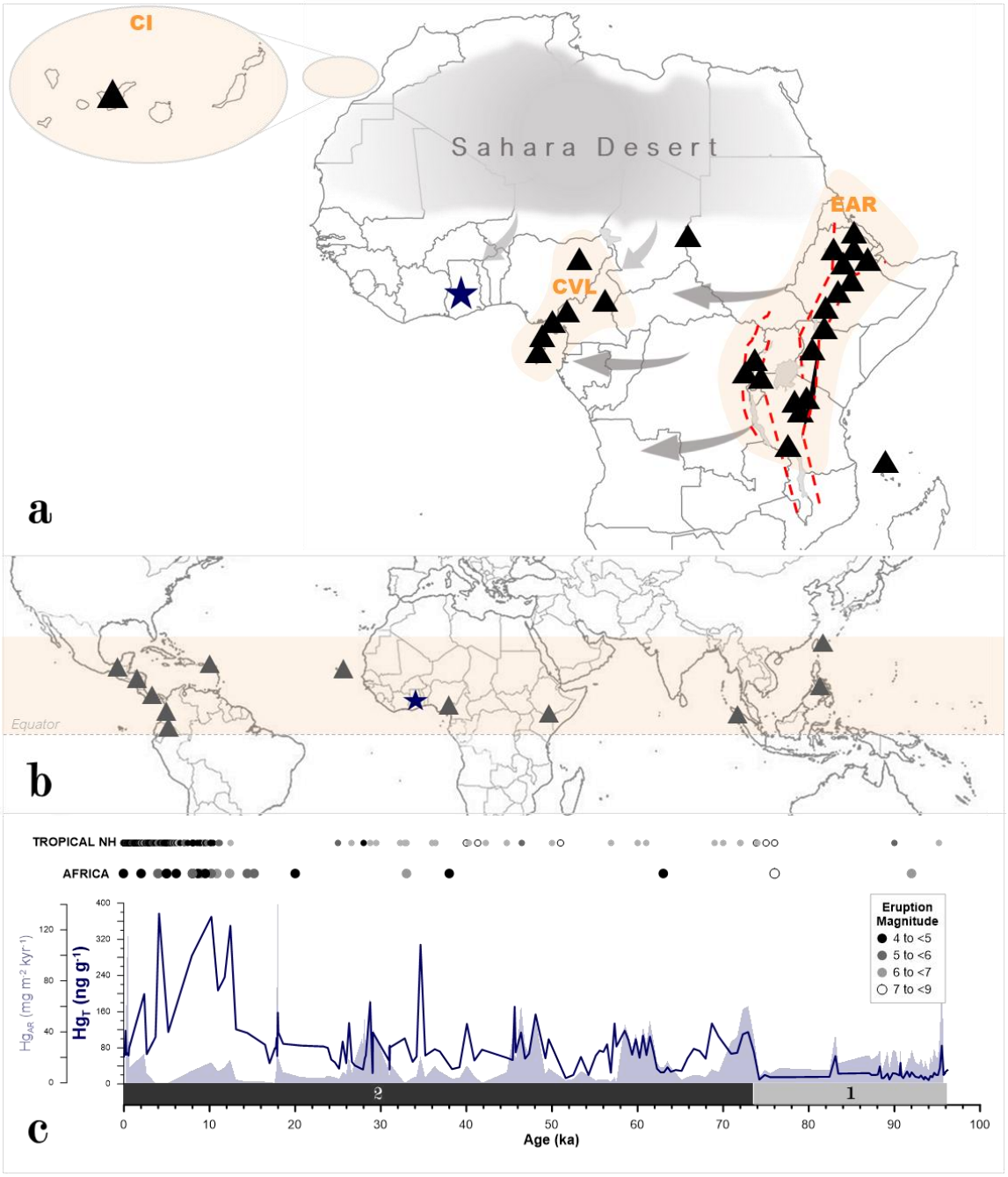

Figure S7: (a) Map of Africa showing volcanic regions with evidence for activity during the late Quaternary (< 100 ka): CI – Canary Islands, CVL – Cameroon Volcanic Line, EAR – East African Rift. Individual systems are marked as grey triangles, and the direction of major atmospheric circulation systems as grey arrows. Lake Bosumtwi is marked as a navy-blue star; (b) Map of the Northern Hemisphere. Black triangles mark volcanic regions possessing known eruptions (>magnitude 4.0) dated between 100–0 ka, as listed in the LaMEVE database (Crosweller et al., 2012). Lake Bosumtwi is marked as a navy-blue star; (c) Time-resolved Hg accumulation rate (Hg_{AR}) and residual Hg (Hg_T) data for BOS04-5B (Lake Bosumtwi) compared to the number and timing of radiometrically-dated eruptions in Africa and the Northern Hemisphere, based on the LaMEVE database and regional tephrostratigraphic records. Circles denoting individual eruptions are coloured with respect to magnitude.

S13. Fire activity

Combustion of terrestrial vegetation is one way catchment-stored Hg may be re-emitted into the atmosphere(Bishop et al., 2020). Typically in its elemental state (Hg_0), Hg retains a low re-volatilisation temperature of 100-300°C(Friedli et al., 2009). Sink capacity varies between different plant species, and so will influence the total amount of Hg released during a wildfire event[3,5]. For example, tropical forest burning makes the greatest contribution to global Hg emissions by wildfire in the post-industrial era (43.3%)(Kumar et al., 2018), and this is likely linked to the greater capacity for tropical plant species to retain high concentrations of Hg(Zhou et al., 2021), elevated litterfall and primary productivity, and/or more frequent fire activity in these regions driven by deforestation(Friedli et al., 2009; Kumar et al., 2018; Melendez-Perez et al., 2014). Enhanced Hg accumulation in forest ecosystems also appears linked to canopy surface area, such that canopy foliage acts as a trap for gaseous and particulate atmospheric mercury with litterfall(Iverfeldt, 1991; Wang et al., 2016; Zhou et al., 2018).

Quantifying the severity, intensity (temperature), and primary fuel source of past fire activity could provide important information regarding wildfire contributions to changes in the terrestrial Hg cycle(Daga et al., 2016; Guédron et al., 2019). Wildfire events are encoded in lake sediment records as discrete layers rich in charcoal particles, produced by the incomplete combustion of organic matter(Whitlock and Larsen, 2002). Charcoal analyses have typically focused on analysis of: (1) microscopic charcoal (<100 μm)(Gosling et al., 2021; Moore et al., 2022; Yost et al., 2018), (2) charcoal abundance by weight calculated by chemical digestion, and/or (3) macroscopic charcoal (>100 μm)(Bonk et al., 2022; Clark and Hussey, 1996; Whitlock and Larsen, 2002). Each proxy can yield a robust record of local and/or regional fire activity on timescales ranging from years, to multiple millennia(Whitlock and Larsen, 2002).

Preliminary macrocharcoal analysis of the BOS04-5B core between 50 and 0 ka suggest that Hg sequestration is not directly coupled to wildfire intensity and/or frequency in Lake Bosumtwi(Kiely, 2023). Linear regression analysis reveals a non-significant relationship between charcoal abundance, maximum fire temperatures, and Hg concentration at Lake Bosumtwi ($P > 0.05$), and Pearson's correlation coefficient measured a similarly negligible correlation between Hg and charcoal abundance and volume (-0.07, -0.1, respectively). **Figure S8** corroborates these results, showing that changes in fire activity do not always correspond to changes in Hg_T or Hg_{AR}. For example, high macrocharcoal particle counts coincide with some of the largest Hg peaks at ~36 ka (**Fig. S8**), whereas fire appears completely absent between 3 and 0 ka: an interval in which the highest Hg concentrations are observed. Moreover, peaks in concentration also often 'lag' behind macrocharcoal enrichments by ~2-kyr (**Fig. S8**), and so whether these two signals are mechanistically linked remains unclear.

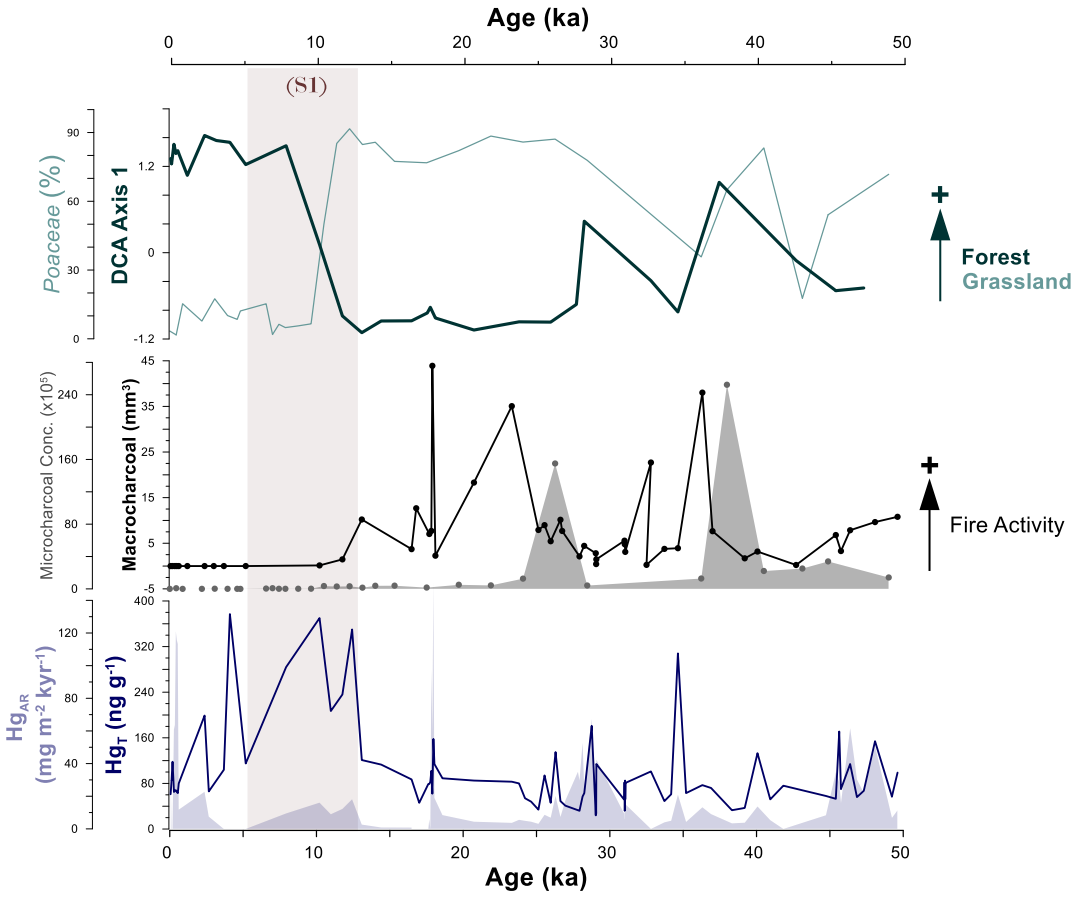

Figure S8: 50-kyr records of total mercury (Hg_T) and mercury accumulation rate (Hg_{AR}) for Lake Bosumtwi from this study, with proxy datasets from prior studies of the same lake. These include forest (woody) taxa abundance represented by detrended correspondence analysis (DCA) axis 1(Gosling et al., 2022; Miller et al., 2016), percentage abundance of Poaceae (grass) pollen(Miller et al., 2016), microcharcoal concentrations(Miller et al., 2016), and macrocharcoal volume(Kiely, 2023). A distinct lake low stand (LS) based on seismic profiles and sedimentological data is marked between 33.5 and 32.8 m depth (grey shading)(Brooks et al., 2005; Scholz et al., 2007), and sapropel layer Unit S1 is marked between 3–5.5 m depth (brown shading)(Shanahan et al., 2012, 2006). Unit AI-1 is marked between 33.5 and 32.8 m depth (grey shading)(Brooks et al., 2005; Scholz et al., 2007), and sapropel layer Unit S1 is marked between 3–5.5 m depth (brown shading)(Shanahan et al., 2012, 2006).

Regional moisture availability is known to broadly modulate vegetation patterns tropical and subtropical systems, and subsequently the expression of fire activity(Gosling et al., 2022; Moore et al., 2022). In the Bosumtwi catchment fire activity also appears correlated to moisture availability(Gosling et al., 2022), with evidence showing elevated charcoal deposition during arid, savannah-dominant intervals, and the reverse during wetter, forest-dominated intervals(Gosling et al., 2021; Miller et al., 2016; Miller and Gosling, 2014). Considering this trend relative to our Hg record, there are several possible reasons for the observed lack of statistical significance between fire severity, intensity and Hg concentration in Lake Bosumtwi: (1) large quantities of particulate-bound Hg were emitted into the atmosphere during arid intervals, but were only deposited into the lake when precipitation was sufficiently heavy (by which point, the primary signal may have disseminated)(Francisco López et al., 2022; Kumar et al., 2018; Melendez-Perez et al., 2014), (2) the

lake's closed structure limited downstream transport of Hg released from burned soils and bound to fine and coarse particulate matter(Bishop et al., 2020; Jensen et al., 2017; Ku et al., 2018), and/or (3) fire-derived Hg signals were overprinted by more dominant processes influencing the sediment record (e.g., primary productivity, detrital mineral supply)(de Lacerda et al., 2017; Paine et al., 2024; Schütze et al., 2018). Although we cannot rule out the possibility that wildfire activity did affect Hg fluxes into the Lake Bosumtwi system, preliminary data suggest that other drivers were likely more influential; namely moisture-driven changes in sedimentation, productivity, and detrital material supply.

References Cited

Armenteros, I., 2010. Diagenesis of Carbonates in Continental Settings, in: Developments in Sedimentology. Elsevier, pp. 61–151. https://doi.org/10.1016/S0070-4571(09)06202-5

Artemieva, N., Morgan, J., Party, E. 364 S., 2017. Quantifying the Release of Climate-Active Gases by Large Meteorite Impacts With a Case Study of Chicxulub. Geophysical Research Letters 44, 10180–10188. https://doi.org/10.1002/2017GL074879

Bahr, D.B., Hutton, E.W.H., Syvitski, J.P.M., Pratson, L.F., 2001. Exponential approximations to compacted sediment porosity profiles. Computers & Geosciences 27, 691–700. https://doi.org/10.1016/S0098-3004(00)00140-0

Biggs, J., Ayele, A., Fischer, T.P., Fontijn, K., Hutchison, W., Kazimoto, E., Whaler, K., Wright, T.J., 2021. Volcanic activity and hazard in the East African Rift Zone. Nature Communications 12, 1–12. https://doi.org/10.1038/s41467-021-27166-y

Bin, C., Xiaoru, W., Lee, F.S.C., 2001. Pyrolysis coupled with atomic absorption spectrometry for the determination of mercury in Chinese medicinal materials. Analytica Chimica Acta 447, 161–169. https://doi.org/10.1016/S0003-2670(01)01218-1

Bishop, K., Shanley, J.B., Riscassi, A., de Wit, H.A., Eklöf, K., Meng, B., Mitchell, C., Osterwalder, S., Schuster, P.F., Webster, J., Zhu, W., 2020. Recent advances in understanding and measurement of mercury in the environment: Terrestrial Hg cycling. Science of the Total Environment 721. https://doi.org/10.1016/j.scitotenv.2020.137647

Blaauw, M., Christen, J.A., 2011. Flexible paleoclimate age-depth models using an autoregressive gamma process. Bayesian Analysis 6, 457–474. https://doi.org/10.1214/11-BA618

Bonk, A., Słowiński, M., Żarczyński, M., Oliński, P., Kupryjanowicz, M., Fiłoc, M., Tylmann, W., 2022. Tracking fire activity and post-fire limnological responses using the varved sedimentary sequence of Lake Jaczno, Poland. The Holocene 32, 515–528. https://doi.org/10.1177/09596836221080755

Brodie, C.R., Leng, M.J., Casford, J.S.L., Kendrick, C.P., Lloyd, J.M., Yongqiang, Z., Bird, M.I., 2011. Evidence for bias in C and N concentrations and δ13C composition of terrestrial and aquatic organic materials due to pre-analysis acid preparation methods. Chemical Geology 282, 67–83. https://doi.org/10.1016/j.chemgeo.2011.01.007

Brooks, K., Scholz, C.A., King, J.W., Peck, J., Overpeck, J.T., Russell, J.M., Amoako, P.Y.O., 2005. Late-Quaternary lowstands of lake Bosumtwi, Ghana: Evidence from high-resolution seismic-reflection and sediment-core data. Palaeogeography, Palaeoclimatology, Palaeoecology 216, 235–249. https://doi.org/10.1016/j.palaeo.2004.10.005

Brown, S.K., Crosweller, H.S., Sparks, R.S.J., Cottrell, E., Deligne, N.I., Guerrero, N.O., Hobbs, L., Kiyosugi, K., Loughlin, S.C., Siebert, L., Takarada, S., 2014. Characterisation of the Quaternary eruption record: Analysis of the Large Magnitude Explosive Volcanic Eruptions (LaMEVE) database. Journal of Applied Volcanology 3, 1–22. https://doi.org/10.1186/2191-5040-3-5

Clark, J.S., Hussey, T.C., 1996. Estimating the mass flux of charcoal from sedimentary records: effects of particle size, morphology, and orientation. The Holocene 6, 129–144. https://doi.org/10.1177/095968369600600201

Colby, D.J., Pyle, D.M., Fontijn, K., Mather, T.A., Melaku, A.A., Mengesha, M.A., Yirgu, G., 2022. Stratigraphy and eruptive history of Corbetti Caldera in the Main Ethiopian Rift. Journal of Volcanology and Geothermal Research 428, 107580. https://doi.org/10.1016/j.jvolgeores.2022.107580

Coney, L., Gibson, R.L., Reimold, W.U., Koeberl, C., 2007. Lithostratigraphic and petrographic analysis of ICDP drill core LB-07A , Bosumtwi impact structure , Ghana 589, 569–589.

Crosweller, H.S., Arora, B., Brown, S.K., Cottrell, E., Deligne, N.I., Guerrero, N.O., Hobbs, L., Kiyosugi, K., Loughlin, S.C., Lowndes, J., Nayembil, M., Siebert, L., Sparks, R.S.J., Takarada, S., Venzke, E., 2012. Global database on large magnitude explosive volcanic eruptions (LaMEVE). Journal of Applied Volcanology 1, 1–13. https://doi.org/10.1186/2191-5040-1-4

Daga, R., Ribeiro Guevara, S., Pavlin, M., Rizzo, A., Lojen, S., Vreča, P., Horvat, M., Arribére, M., 2016. Historical records of mercury in southern latitudes over 1600 years: Lake Futalaufquen, Northern Patagonia. Science of the Total Environment 553, 541–550. https://doi.org/10.1016/j.scitotenv.2016.02.114

de Lacerda, L.D., Turcq, B., Sifeddine, A., Cordeiro, R.C., 2017. Mercury accumulation rates in Caço Lake, NE Brazil during the past 20.000 years. Journal of South American Earth Sciences 77, 42–50. https://doi.org/10.1016/j.jsames.2017.04.008

Deplazes, G., Lückge, A., Peterson, L.C., Timmermann, A., Hamann, Y., Hughen, K.A., Röhl, U., Laj, C., Cane, M.A., Sigman, D.M., Haug, G.H., 2013. Links between tropical rainfall and North Atlantic climate during the last glacial period. Nature Geoscience 6, 213–217. https://doi.org/10.1038/ngeo1712

Edwards, B.A., Kushner, D.S., Outridge, P.M., Wang, F., 2021. Fifty years of volcanic mercury emission research: Knowledge gaps and future directions. Science of the Total Environment 757, 143800. https://doi.org/10.1016/j.scitotenv.2020.143800

Feignon, J.-G., Schulz, T., Ferriere, L., Goderis, S., Claeys, P., Graaff, S.J.D., Kaskes, P., De, T., Koeberl, C., 2022. Search for a meteoritic component within the impact melt rocks of the Chicxulub impact structure peak ring , Mexico. Geochimica et Cosmochimica Acta 323, 74–101. https://doi.org/10.1016/j.gca.2022.02.006

Fendley, I.M., Mittal, T., Sprain, C.J., Marvin-DiPasquale, M., Tobin, T.S., Renne, P.R., 2019. Constraints on the volume and rate of Deccan Traps flood basalt eruptions using a combination of high-resolution terrestrial mercury records and geochemical box models. Earth and Planetary Science Letters 524, 115721. https://doi.org/10.1016/j.epsl.2019.115721

Fitzgerald, W.F., Lamborg, C.H., 2013. Geochemistry of Mercury in the Environment, Treatise on Geochemistry: Second Edition. Elsevier Ltd. https://doi.org/10.1016/B978-0-08-095975-7.00904-9

Fontijn, K., McNamara, K., Zafu Tadesse, A., Pyle, D.M., Dessalegn, F., Hutchison, W., Mather, T.A., Yirgu, G., 2018. Contrasting styles of post-caldera volcanism along the Main Ethiopian Rift: Implications for contemporary volcanic hazards. Journal of Volcanology and Geothermal Research 356, 90–113. https://doi.org/10.1016/j.jvolgeores.2018.02.001

Francisco López, A., Heckenauer Barrón, E.G., Bello Bugallo, P.M., 2022. Contribution to understanding the influence of fires on the mercury cycle: Systematic review, dynamic modelling and application to sustainable hypothetical scenarios. Environ Monit Assess 194, 707. https://doi.org/10.1007/s10661-022-10208-3

Friedli, H.R., Arellano, A.F., Cinnirella, S., Pirrone, N., 2009. Initial estimates of mercury emissions to the atmosphere from global biomass burning. Environmental Science and Technology 43, 3507–3513. https://doi.org/10.1021/es802703g

Gelety, V.F., Kalmykov, G.V., Parkhomenko, I.Y., 2007. Mercury in the sedimentary deposits of Lake Baikal. Geochemistry International 45, 170–177. https://doi.org/10.1134/S001670290702005X

Gosling, W.D., McMichael, C.N.H., Groenwoud, Z., Roding, E., Miller, C.S., Julier, A.C.M., 2021. Preliminary evidence for green, brown and black worlds in tropical western Africa during the Middle and Late Pleistocene. Palaeoecology of Africa 35, 13–25. https://doi.org/10.1201/9781003162766

Gosling, W.D., Miller, C.S., Shanahan, T.M., Holden, P.B., Overpeck, J.T., van Langevelde, Frank., 2022. A stronger role for long-term moisture change than for CO2 in determining tropical woody vegetation change. Science 376, 653–656. https://doi.org/10.1126/science.abg4618

Grant, K.M., Amarathunga, U., Amies, J.D., Hu, P., Qian, Y., Penny, T., Rodriguez-Sanz, L., Zhao, X., Heslop, D., Liebrand, D., Hennekam, R., Westerhold, T., Gilmore, S., Lourens, L.J., Roberts, A.P., Rohling, E.J., 2022. Organic carbon burial in Mediterranean sapropels intensified during Green Sahara Periods since 3.2 Myr ago. Commun Earth Environ 3, 11. https://doi.org/10.1038/s43247-021-00339-9

Grant, K.M., Grimm, R., Mikolajewicz, U., Marino, G., Ziegler, M., Rohling, E.J., 2016. The timing of Mediterranean sapropel deposition relative to insolation, sea-level and African monsoon changes. Quaternary Science Reviews 140, 125–141. https://doi.org/10.1016/j.quascirev.2016.03.026

Grant, K.M., Rohling, E.J., Westerhold, T., Zabel, M., Heslop, D., Konijnendijk, T., Lourens, L., 2017. A 3 million year index for North African humidity/aridity and the implication of potential pan-African Humid periods. Quaternary Science Reviews 171, 100–118. https://doi.org/10.1016/j.quascirev.2017.07.005

Guédron, S., Tolu, J., Brisset, E., Sabatier, P., Perrot, V., Bouchet, S., Develle, A.L., Bindler, R., Cossa, D., Fritz, S.C., Baker, P.A., 2019. Late Holocene volcanic and anthropogenic mercury deposition in the western Central Andes (Lake Chungará Chile). Science of the Total Environment 662, 903–914. https://doi.org/10.1016/j.scitotenv.2019.01.294

Hermanns, Y.M., Biester, H., 2013. A 17,300-year record of mercury accumulation in a pristine lake in southern Chile. Journal of Paleolimnology 49, 547–561. https://doi.org/10.1007/s10933-012-9668-4

Iverfeldt, A., 1991. MERCURY IN FOREST CANOPY THROUGHFALL WATER AND ITS RELATION TO ATMOSPHERIC DEPOSITION. Water Air and Soil Pollution 56, 553–564.

Jenkyns, H.C., 1988. The Early Toarcian (Jurassic) Anoxic Event. American Journal of Science.

Jenkyns, H.C., Weedon, G.P., 2013. Chemostratigraphy (CaCO3, TOC, δ13Corg) of Sinemurian (Lower Jurassic) black shales from the Wessex Basin, Dorset and palaeoenvironmental implications. nos 46, 1–21. https://doi.org/10.1127/0078-0421/2013/0029

Jensen, A.M., Scanlon, T.M., Riscassi, A.L., 2017. Emerging investigator series: The effect of wildfire on streamwater mercury and organic carbon in a forested watershed in the southeastern United States. Environmental Science: Processes and Impacts 19, 1505–1517. https://doi.org/10.1039/c7em00419b

Jourdan, F., Renne, P.R., Reimold, W.U., 2009. An appraisal of the ages of terrestrial impact structures. Earth and Planetary Science Letters 286, 1–13. https://doi.org/10.1016/j.epsl.2009.07.009
Karp, T., Milkereit, B., Janle, P., Danuor, S.K., Pohl, J., Berckhemer, H., Scholz, C.A., 2002. Seismic investigation of the Lake Bosumtwi impact crater: preliminary results. Planetary and Space Science 50, 735–743. https://doi.org/10.1016/S0032-0633(02)00049-1
Kido, Y., Koshikawa, T., Tada, R., 2006. Rapid and quantitative major element analysis method for wet fine-grained sediments using an XRF microscanner. Marine Geology 229, 209–225. https://doi.org/10.1016/j.margeo.2006.03.002
Kiely, R., 2023. A 50,000-year reconstruction of West African fire history (MSc Thesis). University of Amsterdam, Amsterdam.
Kinsley, C.W., Bradtmiller, L.I., McGee, D., Galgay, M., Stuut, J.B., Tjallingii, R., Winckler, G., DeMenocal, P.B., 2022. Orbital and Millennial-Scale Variability in Northwest African Dust Emissions Over the Past 67,000 years. Paleoceanography and Paleoclimatology 37, 1–22. https://doi.org/10.1029/2020PA004137
Koeberl, C., Bottomley, R., Glass, B.P., Storzer, D., 1997. Geochemistry and age of Ivory Coast tektites and microtektites. Geochimica et Cosmochimica Acta 61, 1745–1772. https://doi.org/10.1016/S0016-7037(97)00026-4
Koeberl, C., Brandstätter, F., Glass, B.P., Hecht, L., Mader, D., Reimold, W.U., 2007a. Uppermost impact fallback layer in the Bosumtwi crater (Ghana): Mineralogy, geochemistry, and comparison with Ivory Coast tektites. Meteoritics and Planetary Science 42, 709–729. https://doi.org/10.1111/j.1945-5100.2007.tb01069.x
Koeberl, C., Milkereit, B., Overpeck, J.T., Scholz, C.A., Amoako, P.Y.O., Boamah, D., Danuor, S.K., Karp, T., Kueck, J., Hecky, R.E., King, J.W., Peack, J.A., 2007b. An international and multidisciplinary drilling project into a young complex impact structure: The 2004 ICDP Bosumtwi Crater Drilling Project - An overview. Meteoritics and Planetary Science 42, 483–511. https://doi.org/10.1111/j.1945-5100.2007.tb01057.x
Koeberl, C., Peck, J., King, J., Milkereit, B., Overpeck, J., Scholz, C., 2005. The ICDP lake Bosumtwi drilling project: A first report. Scientific Drilling 1, 23–27. https://doi.org/10.2204/iodp.sd.1.04.2005
Ku, P., Tsui, M.T.-K., Nie, X., Chen, H., Hoang, T.C., Blum, J.D., Dahlgren, R.A., Chow, A.T., 2018. Origin, Reactivity, and Bioavailability of Mercury in Wildfire Ash. Environ. Sci. Technol. 52, 14149–14157. https://doi.org/10.1021/acs.est.8b03729
Kumar, A., Wu, S., Huang, Y., Liao, H., Kaplan, J.O., 2018. Mercury from wildfires: Global emission inventories and sensitivity to 2000–2050 global change. Atmospheric Environment 173, 6–15. https://doi.org/10.1016/j.atmosenv.2017.10.061
Lane, C.S., Chorn, B.T., Johnson, T.C., 2013. Ash from the Toba supereruption in Lake Malawi shows no volcanic winter in East Africa at 75 ka. Proceedings of the National Academy of Sciences 110. https://doi.org/10.1073/pnas.1301474110
McKay, N.P., 2012. A multidisciplinary approach to late Quaternary paleoclimatology with an emphasis on sub-saharan West Africa and the last interglacial period (PhD Thesis). University of Arizona, Arizona.
Melendez-Perez, J.J., Fostier, A.H., Carvalho, J.A., Windmöller, C.C., Santos, J.C., Carpi, A., 2014. Soil and biomass mercury emissions during a prescribed fire in the Amazonian rain forest. Atmospheric Environment 96, 415–422. https://doi.org/10.1016/j.atmosenv.2014.06.032
Miller, C.S., Gosling, W.D., 2014. Quaternary forest associations in lowland tropical West Africa. Quaternary Science Reviews 84, 7–25. https://doi.org/10.1016/j.quascirev.2013.10.027
Miller, C.S., Gosling, W.D., Kemp, D.B., Coe, A.L., Gilmour, I., 2016. Drivers of ecosystem and climate change in tropical West Africa over the past ~540 000 years. Journal of Quaternary Science 31, 671–677. https://doi.org/10.1002/jqs.2893
Moore, H.R., Crocker, A.J., Belcher, C.M., Meckler, A.N., Osborne, C.P., Beerling, D.J., Wilson, P.A., 2022. Hydroclimate variability was the main control on fire activity in northern Africa over the last 50,000 years. Quaternary Science Reviews 288, 107578. https://doi.org/10.1016/j.quascirev.2022.107578
Oehlert, A.M., Swart, P.K., 2019. Rolling window regression of $\delta^{13}C$ and $\delta^{18}O$ values in carbonate sediments: Implications for source and diagenesis. Depositional Rec 5, 613–630. https://doi.org/10.1002/dep2.88
Paine, A.R., Fendley, I.M., Frieling, J., Mather, T.A., Lacey, J.H., Wagner, B., Robinson, S.A., Pyle, D.M., Francke, A., Them II, T.R., Panagiotopoulos, K., 2024. Mercury records covering the past 90 000 years from lakes Prespa and Ohrid, SE Europe. Biogeosciences 21, 531–556. https://doi.org/10.5194/bg-21-531-2024
Pérez-Rodríguez, M., Biester, H., Aboal, J.R., Toro, M., Martínez Cortizas, A., 2019. Thawing of snow and ice caused extraordinary high and fast mercury fluxes to lake sediments in Antarctica. Geochimica et Cosmochimica Acta 248, 109–122. https://doi.org/10.1016/j.gca.2019.01.009
Pyle, D.M., 1999. Widely dispersed Quaternary tephra in Africa. Global and Planetary Change 21, 95–112. https://doi.org/10.1016/S0921-8181(99)00009-0
Pyle, D.M., Mather, T.A., 2003. The importance of volcanic emissions for the global atmospheric mercury cycle. Atmospheric Environment 37, 5115–5124. https://doi.org/10.1016/j.atmosenv.2003.07.011
Ribeiro Guevara, S., Meili, M., Rizzo, A., Daga, R., Arribére, M., 2010. Sediment records of highly variable mercury inputs to mountain lakes in patagonia during the past millennium. Atmospheric Chemistry and Physics 10, 3443–3453. https://doi.org/10.5194/acp-10-3443-2010
Rytuba, J.J., 2003. Mercury from mineral deposits and potential environmental impact. Environmental Geology 43, 326–338. https://doi.org/10.1007/s00254-002-0629-5

Schlüter, K., 2000. Review: Evaporation of mercury from soils. An integration and synthesis of current knowledge. Environmental Geology 39, 249–271. https://doi.org/10.1007/s002540050005
Scholz, C.A., Johnson, T.C., Cohen, A.S., King, J.W., Peck, J.A., Overpeck, J.T., Talbot, M.R., Brown, E.T., Kalindekafe, L., Amoako, P.Y.O., Lyons, R.P., Shanahan, T.M., Castañeda, I.S., Heil, C.W., Forman, S.L., McHargue, L.R., Beuning, K.R., Gomez, J., Pierson, J., 2007. East African megadroughts between 135 and 75 thousand years ago and bearing on early-modern human origins. Proceedings of the National Academy of Sciences of the United States of America 104, 16416–16421. https://doi.org/10.1073/pnas.0703874104
Schütze, M., Tserendorj, G., Pérez-Rodríguez, M., Rösch, M., Biester, H., 2018. Prediction of Holocene mercury accumulation trends by combining palynological and geochemical records of lake sediments (Black Forest, Germany). Geosciences (Switzerland) 8. https://doi.org/10.3390/geosciences8100358
Sebag, D., Garcin, Y., Adatte, T., Deschamps, P., Ménot, G., Verrecchia, E.P., 2018. Correction for the siderite effect on Rock-Eval parameters: Application to the sediments of Lake Barombi (southwest Cameroon). Organic Geochemistry 123, 126–135. https://doi.org/10.1016/j.orggeochem.2018.05.010
Selin, N.E., 2009. Global biogeochemical cycling of mercury: a review. Annual Review of Environmental Resources 34, 43–63.
Shanahan, T.M., Beck, J.W., Overpeck, J.T., McKay, N.P., Pigati, J.S., Peck, J.A., Scholz, C.A., Heil, C.W., King, J., 2012. Late Quaternary sedimentological and climate changes at Lake Bosumtwi Ghana: New constraints from laminae analysis and radiocarbon age modeling. Palaeogeography, Palaeoclimatology, Palaeoecology 361–362, 49–60. https://doi.org/10.1016/j.palaeo.2012.08.001
Shanahan, T.M., Overpeck, J.T., Wheeler, C.W., Beck, J.W., Pigati, J.S., Talbot, M.R., Scholz, C.A., Peck, J., King, J.W., 2006. Paleoclimatic variations in West Africa from a record of late Pleistocene and Holocene lake level stands of Lake Bosumtwi, Ghana. Palaeogeography, Palaeoclimatology, Palaeoecology 242, 287–302. https://doi.org/10.1016/j.palaeo.2006.06.007
Shanahan, T.M., Peck, J.A., McKay, N., Heil, C.W., King, J., Forman, S.L., Hoffmann, D.L., Richards, D.A., Overpeck, J.T., Scholz, C., 2013. Age models for long lacustrine sediment records using multiple dating approaches - An example from Lake Bosumtwi, Ghana. Quaternary Geochronology 15, 47–60. https://doi.org/10.1016/j.quageo.2012.12.001
Skonieczny, C., McGee, D., Winckler, G., Bory, A., Bradtmiller, L.I., Kinsley, C.W., Polissar, P.J., De Pol-Holz, R., Rossignol, L., Malaizé, B., 2019. Monsoon-driven Saharan dust variability over the past 240,000 years. Science Advances 5, 1–9. https://doi.org/10.1126/sciadv.aav1887
Sun, Y., McManus, J.F., Clemens, S.C., Zhang, X., Vogel, H., Hodell, D.A., Guo, F., Wang, T., Liu, X., An, Z., 2021. Persistent orbital influence on millennial climate variability through the Pleistocene. Nature Geoscience 14, 812–818. https://doi.org/10.1038/s41561-021-00794-1
Tjallingii, R., Claussen, M., Stuut, J.-B.W., Fohlmeister, J., Jahn, A., Bickert, T., Lamy, F., Röhl, U., 2008. Coherent high- and low-latitude control of the northwest African hydrological balance. Nature Geosci 1, 670–675. https://doi.org/10.1038/ngeo289
Ulfers, A., Zeeden, C., Voigt, S., Sardar Abadi, M., Wonik, T., 2022. Half-precession signals in Lake Ohrid (Balkan) and their spatio-temporal relations to climate records from the European realm. Quaternary Science Reviews 280, 107413. https://doi.org/10.1016/j.quascirev.2022.107413
United Nations Environment Programme, 2018. Global Mercury Assessment, United Nations.
Vidal, C.M., Fontijn, K., Lane, C.S., Asrat, A., Barfod, D., Tomlinson, E.L., Piermattei, A., Hutchison, W., Tadesse, A.Z., Yirgu, G., Deino, A., Moussallam, Y., Mohr, P., Williams, F., Mather, T.A., Pyle, D.M., Oppenheimer, C., 2022. Geochronology and glass geochemistry of major Pleistocene eruptions in the Main Ethiopian Rift: Towards a regional tephrostratigraphy. Quaternary Science Reviews 290, 107601. https://doi.org/10.1016/j.quascirev.2022.107601
Vindušková, O., Jandová, K., Frouz, J., 2019. Improved method for removing siderite by *in situ* acidification before elemental and isotope analysis of soil organic carbon. J. Plant Nutr. Soil Sci. 182, 82–91. https://doi.org/10.1002/jpln.201800164
Wang, X., Bao, Z., Lin, C.-J., Yuan, W., Feng, X., 2016. Assessment of Global Mercury Deposition through Litterfall. Environ. Sci. Technol. 50, 8548–8557. https://doi.org/10.1021/acs.est.5b06351
Wang, X., Piao, S., Ciais, P., Friedlingstein, P., Myneni, R.B., Cox, P., Heimann, M., Miller, J., Peng, S., Wang, T., Yang, H., Chen, A., 2014. A two-fold increase of carbon cycle sensitivity to tropical temperature variations. Nature 506, 212–215. https://doi.org/10.1038/nature12915
Weldeab, S., Lea, D.W., Schneider, R.R., Andersen, N., 2007. 155,000 Years of West African Monsoon and Ocean Thermal Evolution. Science 316, 1303–1307. https://doi.org/10.1126/science.1140461
Whitlock, C., Larsen, C., 2002. Charcoal as a Fire Proxy, in: Smol, J.P., Birks, H.J.B., Last, W.M., Bradley, R.S., Alverson, K. (Eds.), Tracking Environmental Change Using Lake Sediments, Developments in Paleoenvironmental Research. Springer Netherlands, Dordrecht, pp. 75–97. https://doi.org/10.1007/0-306-47668-1_5
Yost, C.L., Jackson, L.J., Stone, J.R., Cohen, A.S., 2018. Subdecadal phytolith and charcoal records from Lake Malawi , East Africa imply minimal effects on human evolution from the ~ 74 ka Toba supereruption. Journal of Human Evolution 116, 75–94. https://doi.org/10.1016/j.jhevol.2017.11.005
Zhou, J., Obrist, D., Dastoor, A., Jiskra, M., Ryjkov, A., 2021. Vegetation uptake of mercury and impacts on global cycling. Nature Reviews Earth and Environment 2, 269–284. https://doi.org/10.1038/s43017-021-00146-y

Zhou, J., Wang, Z., Zhang, X., 2018. Deposition and Fate of Mercury in Litterfall, Litter, and Soil in Coniferous and Broad-Leaved Forests. Journal of Geophysical Research: Biogeosciences 123, 2590–2603. https://doi.org/10.1029/2018JG004415